Size-dependent melting of Bi nanoparticles

E. A. Olson,[a] M. Yu. Efremov, M. Zhang, Z. Zhang, and L. H. Allen[b]
Coordinated Science Laboratory, Department of Materials Science and Engineering, University of Illinois at Urbana–Champaign, Urbana, Illinois, 61801

(Received 13 April 2004; accepted 19 October 2004; published online 6 January 2005)

Nanocalorimetry was used to investigate the melting of Bi nanoparticles. The particles were formed by evaporating Bi onto a silicon nitride substrate, which was then heated. The particles self-assemble into truncated spherical particles. Below 5-nm average film thickness, mean particle sizes increased linearly with deposition thickness but increased rapidly for 10-nm-thick films. As expected, small particles were found to exhibit size-dependent melting temperatures less than the bulk melting temperature (e.g., $\Delta T=67$ K for a 3-nm radius particle). The measured melting temperatures for particles below ~7 nm in radius, however, were ~50 K above the value predicted by the homogeneous melting model. We discuss this discrepancy in terms of a possible size-dependent crystal structure change and the superheating of the solid phase. © *2005 American Institute of Physics*. [DOI: 10.1063/1.1832741]

I. INTRODUCTION

The effect of surfaces and interfaces on bulk material properties can become dominant in nanometer-sized samples of materials. In a macroscopic sample, these surfaces and interfaces are usually proportionately so small that they have only a small effect on the overall properties of a material. At the nanoscale, however, they can be a large fraction of the material sample itself. The ever-increasing desire to work with materials in smaller and smaller amounts requires a thorough understanding of the size effects on material properties.

The electronic properties of bismuth have been an object of study for a number of reasons, including its highly anisotropic electron and hole effective masses,[1] and high values for its electron mean free path and mobility.[2] It is a prominent material for thermoelectric applications.[3] It has more recently become of interest due to its ability to form nanowires, nanotubes, and epitaxial nanolines on Si.[4]

The phenomenon of melting point depression (a melting temperature smaller than the bulk) in small bismuth particles was observed some time ago.[5,6] Melting point depression, theorized by Pawlow[7] in 1909, is due to the large influence of the surface energy on the properties of small particles. Such forces are generally negligible in the bulk, but at the nanoscale, surface-to-volume ratios become very high. Surface effects can become dominant and change material properties from their macroscopic, bulk values.

There are a number of different theories of how the melting of small particles proceeds. Usually such models incorporate elements such as a quasiliquid layer covering the surface of the particle below its melting temperature, or the nucleation and growth of the liquid at the surface,[8] which grows as the particle melts. Couchman and Ryan hypothesized that melting occurs when the rms vibrational displacement of an atom reaches a critical fraction of the interatomic spacing.[9] Most models generally predict melting temperatures that will follow the form

$$\Delta T = T_m^{\text{bulk}} - T_m(r) = \left(\frac{2T_m^{\text{bulk}}}{H_m^{\text{bulk}}\rho_S}\right)\left(\frac{\alpha}{r}\right) = \frac{A}{r}, \tag{1}$$

where T_m^{bulk} is the bulk melting temperature, $T_m(r)$ is the size-dependent melting temperature, H_m^{bulk} is the bulk heat of fusion, ρ_S is the solid phase density, r is the radius, and A is a constant.[10,11] The parameter α depends on the melting model. An excellent review article on cluster melting has been written by Schmidt and Haberland.[11] Berry has written extensively on the idea of the coexistence of multiple phases in finite-sized clusters.[12]

There is little evidence for a quasiliquid layer on the surface of small Bi particles, as opposed to other material systems [e.g., Sn and Pb (Refs. 13–15)], so the homogenous melting model (HMM) is usually applied. The HMM assumes that a particle melts completely when it reaches its melting temperature and there is no premelting. The parameter α for this model can be determined by

$$\alpha_{\text{HMM}} = \sigma_{\text{SV}} - \sigma_{\text{LV}}\left(\frac{\rho_S}{\rho_L}\right)^{2/3}, \tag{2}$$

where σ_{SV} is the interface energy of the solid-vapor interface (a difficult parameter to obtain experimentally for most solids), σ_{LV} is the energy of the liquid-vapor interface, and ρ_L is the liquid phase density. Using the values found in Table I,

TABLE I. Some material properties of Bi (see Ref. 6).

Constant	Value
T_m^{bulk}	544.4 K
H_m^{bulk}	51.9 J/g
σ_{SV}	550 mJ/m^2
σ_{LV}	375 mJ/m^2
ρ_S	9.8 g/cm^3
ρ_L	10.1 g/cm^3

[a]Electronic mail: olson@mrl.uiuc.edu
[b]Author to whom correspondence should be addressed; electronic mail: l-allen9@uiuc.edu

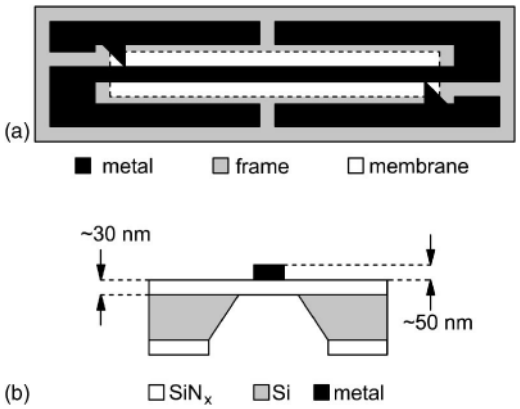

FIG. 1. Nanocalorimetric sensor schematic, not to scale. (a) Top view, showing the metal heater layer, the supporting frame, and the ultrathin membrane. (b) Cross-section view. The sample (not shown) is usually deposited on the SiN_x face of the membrane and directly opposite the metal heater.

$\alpha_{HMM}=181$ mJ/m^2 and $A=388$ nm K in Eq. (1).

In this paper we report our results of a transmission electron microscopy (TEM) and calorimetric study on the growth and melting properties of small particles of Bi. We find the unexpected result that particles of sizes below 7-nm radius melt at ~50 K above the temperature as predicted by Eq. (1).

II. EXPERIMENT

Nanocalorimetry relies on microfabrication to reduce the size and heat capacity of thermal sensors to the point where they are on the scale of the sample itself. This is done by using an ~50-nm-thick silicon nitride (SiN_x) membrane for mechanical support and an ~50-nm-thick metal film as a heater and resistive thermometer. The thin-film nature of the sensor keeps its total heat capacity (the addenda) low. Details of the sensor design and fabrication as well as the experimental procedure are described in detail elsewhere.[10,16] A schematic of a nanocalorimetric sensor is shown in Fig. 1.

Bi films are deposited on the SiN_x membrane by thermal evaporation. A shadow mask is used to constrain the deposition only to the area of the SiN_x membrane measured by the temperature sensor. The total area of the sensor is 2.9 mm^2, and the area of deposition exposed by the shadow mask is 2.5 mm^2. The base pressure of the vacuum system is $\sim 5\times10^{-8}$ torr and increases to $\sim 1\times10^{-7}$ torr during evaporation.

At this base pressure, we estimate that the time needed for a monolayer of gas to adsorb to the surface is greater than 30 s.[17] We begin the calorimetry only a few seconds after finishing the deposition to minimize the adsorbed gas and the formation of the native oxide.

We encountered one particular experimental challenge in Bi evaporation that we did not observe in previous experiments with In and Sn. Instead of Bi being deposited only on the SiN_x side of the sensor, Bi was also simultaneously deposited (in smaller amounts) on the metal heater side of the sensor, which faced away from the evaporation source. We speculate that this occurs because evaporated Bi vapor (probably in the form of molecules of a few atoms) can undergo multiple adsorption and desorption events inside the vacuum chamber and deposit on the surfaces that do not have a line-of-sight to the evaporative source. Even a small amount of Bi deposited on the Au metal areas of the sensor results in a strong, deleterious effect on its electrical characteristics. This effect compromises the measured value of the resistance R, and therefore, the temperature T, since T is calculated from the measured R. For a sensor with a Au metallization, this is seen through an increase in the room-temperature resistance. This effect occurs even though the SiN_x surface of the sensor is shielded from the line-of-sight deposition by a shutter. The increase in resistance was proportional to the amount of Bi evaporated in the chamber. Bi contamination on the Au surface was confirmed by Auger spectroscopy. To eliminate this effect, a box was constructed to enclose the sensors during experiments. Small holes were used so the box could be evacuated. This prevents Bi from interacting with the sensor. Thereafter, no measured change in the room-temperature resistance of the sensors even for thick, heavy Bi depositions was observed.

During a calorimetric pulse, a dc electrical pulse is applied to the heater. Resistive heating causes the temperature of the system to increase. By measuring the electrical power P and the temperature T as functions of time t, the heat capacity C_P of the entire system can be determined. As a first approximation, this is given by

$$C_P = \frac{dQ}{dT} = \frac{dQ}{dt}\frac{dt}{dT} = P(t)\left(\frac{dT}{dt}\right)^{-1}, \tag{3}$$

where Q is the heat input to the system.

The heating rates (dT/dt) used in a nanocalorimetric experiment are high to keep the experimental conditions close to the adiabatic. Heating rates can range between 5 and 1000 kK/s, with a typical heating rate of ~30 kK/s. This is much higher than those used in a conventional differential scanning calorimetry (DSC), which uses heating rates of ~1 K/s. After the end of the pulse, the samples cool passively at an initial rate of ~6 kK/s.

Since the SiN_x membrane is thin, TEM can be performed directly through it. From TEM micrographs, a particle size distribution can be determined. Once this distribution is combined with $C_P(T)$ information from the calorimetry, the size-dependent melting temperature $T_m(r)$ can be determined.[10]

III. RESULTS

A. Bi growth characteristics and TEM

In the early stages of deposition (under 10-nm total thickness), the size of melted particles gradually increases. In the as-deposited state, thin films consist of small, two-dimensional, irregularly shaped, faceted platelets. Upon melting, the material forms truncated spheres (islands). Cooling and subsequent pulsing do not significantly change the shape of the particles after the first few pulses. This can be seen in Fig. 2 for both In and Bi. A Bi film, which is nominally 5 nm thick, in its as-deposited (cold) state, consists of polygonal platelets [Fig. 2(a)]. After pulsing, the particles exhibit circular projected areas in plan view TEM micrographs [Fig. 2(b)].

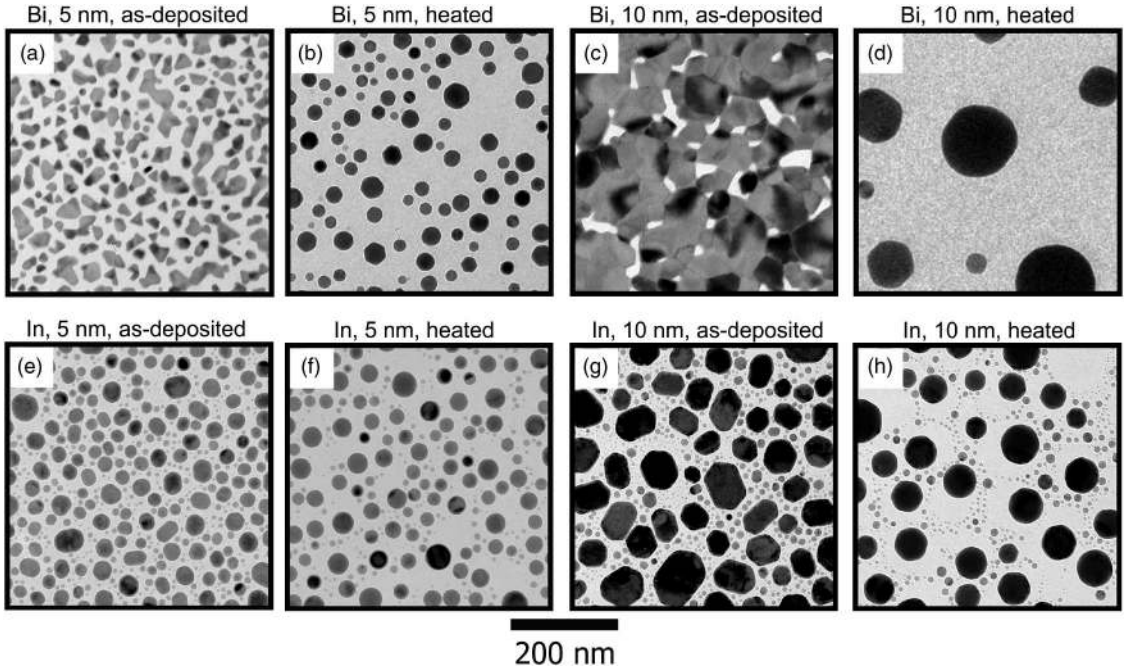

FIG. 2. Bright-field TEM micrographs for Bi and In films of two different thicknesses, showing the effect of heating. (a) Unheated Bi film, 5 nm thick, made up of unconnected, polygonal particles. (b) Another 5–nm Bi film, after being heated above T_m^{bulk}. (c) Unheated 10–nm Bi film. Here, the film has formed an interconnected network. (d) Heated 10–nm Bi film. The particle size has increased dramatically over the heated 5–nm film, and the particles are also larger than in the heated In film of the same nominal thickness. (e) Unheated 5–nm In film. (f) Heated 5–nm In film. (g) Unheated 10–nm In film. (h) Heated 10–nm In film.

At higher thicknesses, the films become percolated [see the 10-nm film in Fig. 2(c)]. Upon melting, these percolated films form islands much larger than expected [Fig. 2(d)]. This effect is only observed if the as-deposited platelets percolate and form an interconnecting network prior to melting. Figure 3 shows the mean particle radius versus the nominal film thickness for heated Bi, In, and Sn films. Below ~5 nm, all three materials behave approximately the same. However, at 10 nm thick, a Bi film shows a much larger (2.4×) average particle radius than an In film of similar thickness. Comparisons of Bi with In and Sn are made often throughout this paper because of our previous work in size-dependent effects using TEM and calorimetry,[10,18] using similar equipment and techniques.

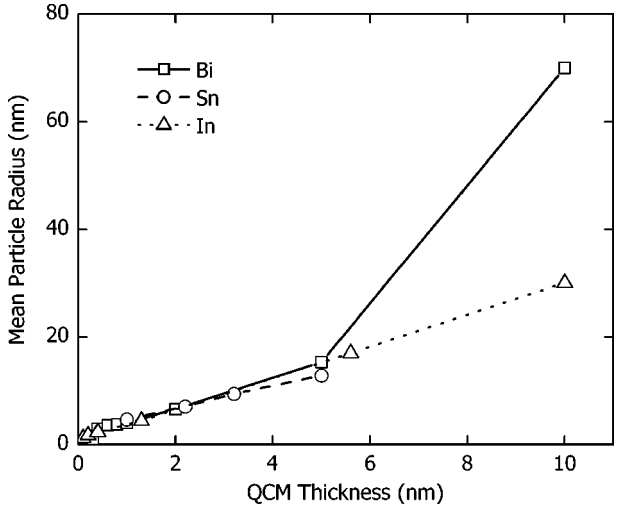

FIG. 3. Mean particle radius vs average film thickness for Bi, In, and Sn. Data for Sn films above 5 nm were not available. Note that, at 10 nm, the Bi islands are 2× larger than the In islands, even though the same amount of material was deposited. We speculate that this occurs because unheated Bi films are an interconnected network at 10-nm film thickness, while In films are still composed of individual particles, as can be seen in Fig. 2.

We can exploit the effect of the percolated films forming very large islands to create bimodal distributions of particle size, as can be seen in Fig. 4. This is done by performing the evaporation in two steps. First, a 10-nm Bi is deposited and then heated to form large particles with radii of ~70 nm. Then, an additional 0.8-nm Bi is deposited and heated to form small particles with radii of ~5 nm. A TEM micrograph of one such film can be seen in Fig. 4(a). The heat capacity for these films before and after the 0.8-nm Bi deposition is shown in Fig. 4(b).

Size distribution histograms of the two films can be seen in Figs. 4(c) and 4(d). The histograms are obtained by an image analysis of bright-field TEM micrographs (SCION IMAGE, Scion Corp.) In these figures, the *y*-axis value for each histogram bin has been multiplied by the volume of the particles in that bin $\left(V=\frac{4}{3}\pi r^3\right)$ so that it reflects the fraction of the total volume of Bi deposited. It has also been divided by the size of the histogram bin, and so the *y* axis is unitless. See Ref. 10 for details.

As expected, the additional 0.8-nm deposition does not significantly modify the large melting peak at 260 °C. Instead, the smaller radii of the second set of particles and the size dependence of T_m create a second melting peak at ~225 °C, which is consistent with single-evaporation experiments (see Fig. 8). We have observed bimodal melting in

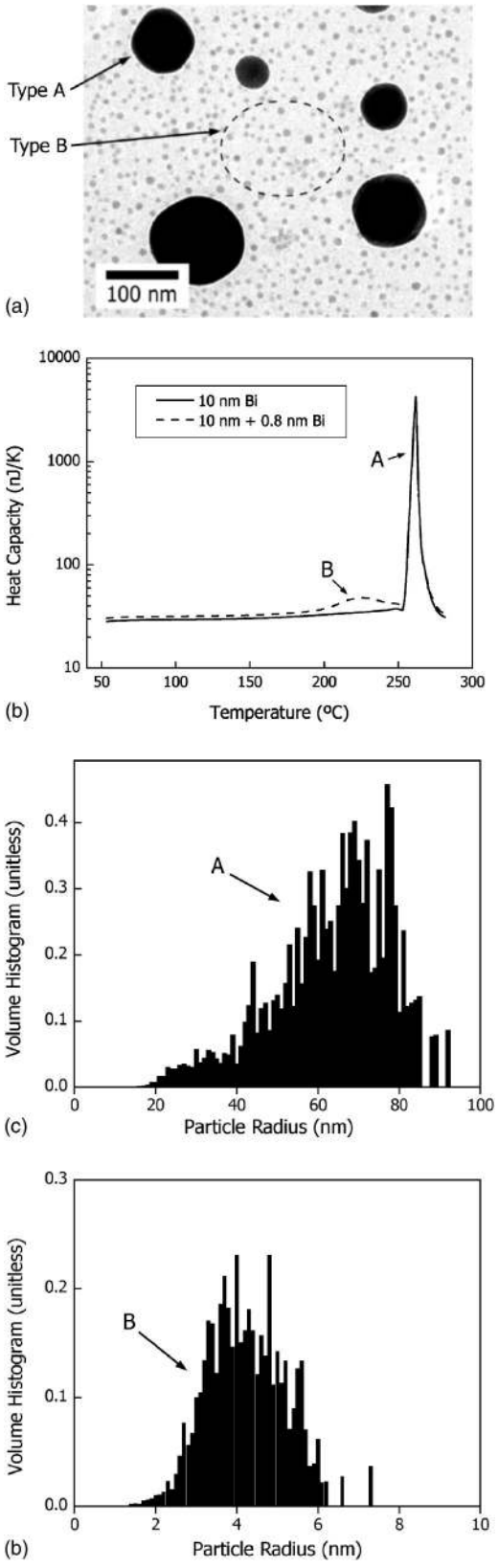

FIG. 4. Results from a two-step deposition, which created a bimodal particle size distribution. A 10-nm Bi deposition was made in order to form large particles, then an additional 0.8 nm deposited to form small ones. (a) A TEM micrograph showing a few very large particles combined with many smaller ones. (b) Heat-capacity data from the 10- and the 10+0.8-nm films. The smaller particles have a lower T_m, which can be seen in the small melting peak at ~225 °C. (c) Size distribution histogram for a 10-nm deposition. (d) The low-radius section of a size distribution histogram for a 10 +0.8-nm film.

such a nanoparticle system. This phenomenon may be exploited in future experiments as a form of internal temperature calibration.

B. Calorimetry

Heat capacity for three Bi films can be seen in Fig. 5, along with TEM micrographs for each film.[19] Melting point depression is clearly seen. The thickest film, at 2.0-nm nominal thickness, has large particles and, as expected, a higher average melting temperature. The 0.6-nm film has smaller particles and the average melting temperature is lower. The 0.3-nm film has the smallest particles and the lowest melting temperature. Latent heat of melting, represented as the area under the melting peak, similarly decreases with the material deposited. Since there is less material in the 0.3-nm film than those in the others, its latent heat is also smaller, and the integrated area under the peak is smaller. The melting peak becomes increasingly broad as the average size of the particles decreases. This is expected, since there is a wide distribution of particle size. The smaller-sized end of the distribution melts at lower temperatures than the larger-sized end. We would prefer uniform particles of a single size, but this cannot be achieved by this method of particle preparation.

A quartz-crystal monitor (QCM) is used to measure the nominal film thickness during deposition. However, at low deposition amounts (<1 nm) the QCM can seriously overestimate the thickness of Bi that is actually deposited on the sensor. To obtain an accurate value of the amount of Bi deposited on the sensor, we use the heat-capacity measurement by monitoring the change in the C_P base line.[20] Since the specific heat of Bi is not expected to be size dependent at these sizes,[21] it will be proportional to the mass of material deposited on the sensor surface. The mass can be calculated by[22]

$$m = \frac{C_P(T)}{\overline{c_P}(T)}, \tag{4}$$

where m is the mass of the deposited sample and $\overline{c_p}(T)$ is the bulk specific heat (i.e., heat capacity per gram) of the sample substance. For Bi,[23] $\overline{c_P}$=0.12 J g^{-1} K^{-1} at 25 °C. This is illustrated in Fig. 5.

The measured heat capacity at 50 °C is determined by a least-squares linear fit to the data between 40 and 60 °C. This value is compared with the QCM thickness (i.e., mass) in Fig. 6. Note the large deviation from the expected linear relationship (dashed line) at low amounts of Bi. We deduce that at the early stages (<0.1 nm) of deposition, Bi accumulates at a much lower rate on the calorimeter as compared with the QCM. This is not surprising since the mechanics of growth are much different for the two systems. In the case of the QCM, the situation is straightforward: it has been uniformly coated with large amounts of Bi during the initial part of an experiment, in which a stable rate of Bi evaporation is established while the shutter is still closed. However, in the case of the calorimeter at the initial stages of deposition, the Bi impinges onto an inert SiN_x surface, which we expect involves a lower Bi–SiN_x sticking coefficient compared to the Bi–Bi sticking coefficient of the QCM. Furthermore, Bi

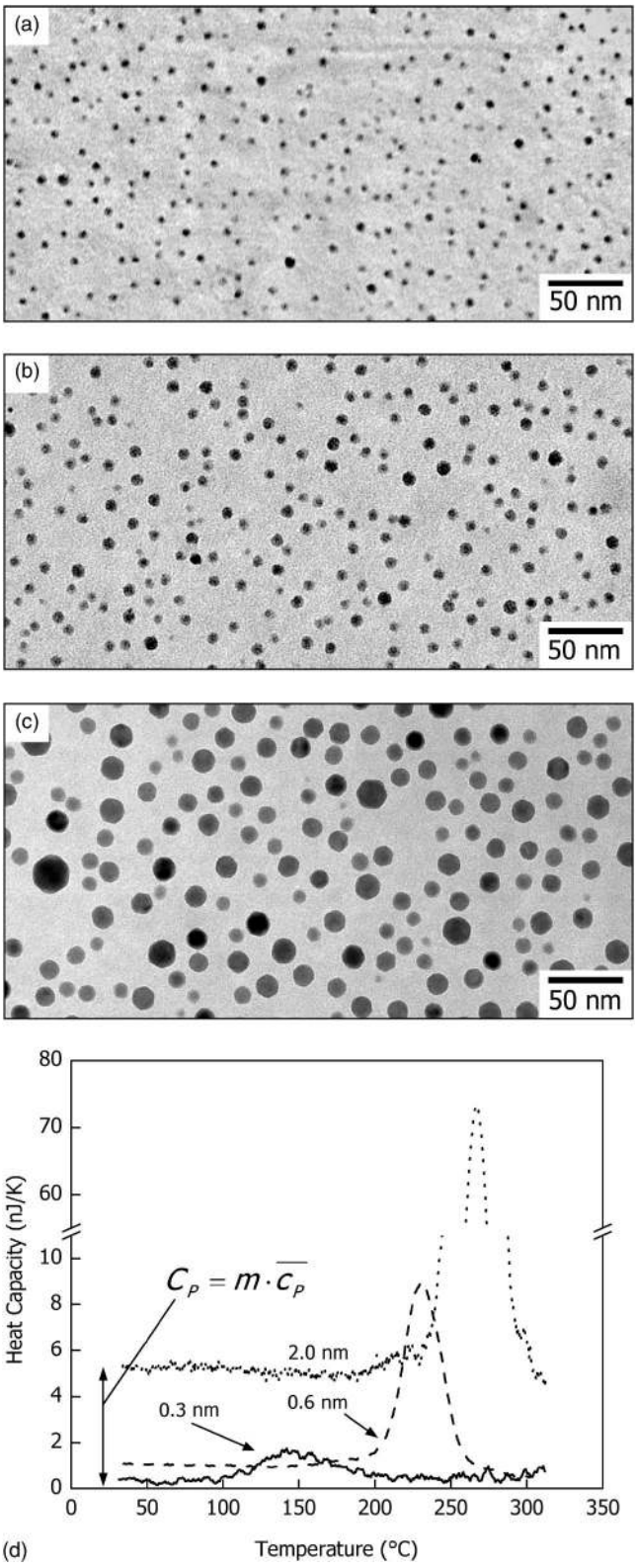

FIG. 5. TEM micrographs and $C_P(T)$ curves for three different Bi films. Top to bottom, the micrographs are of heated Bi films with nominal thicknesses of 0.3, 0.6, and 2.0 nm thick. Particles get larger as the total deposition increases, and the melting temperature increases with the increasing size. Base line C_P also increases, as the total deposited mass increases with thickness. In other words, $C_P = m(\overline{c_P})$.

accumulation on the sensor requires lateral surface diffusion to form islands (unlike the accumulation process on the QCM), a process that allows additional time for Bi desorption from the SiN_x surface. The difference in the measurement of the Bi mass is even more dramatic during real-time, *in situ* C_P measurements, in which the sensor is repeatedly pulsed during deposition. In this case, the QCM overestimates the amount of Bi by a factor of 50×.

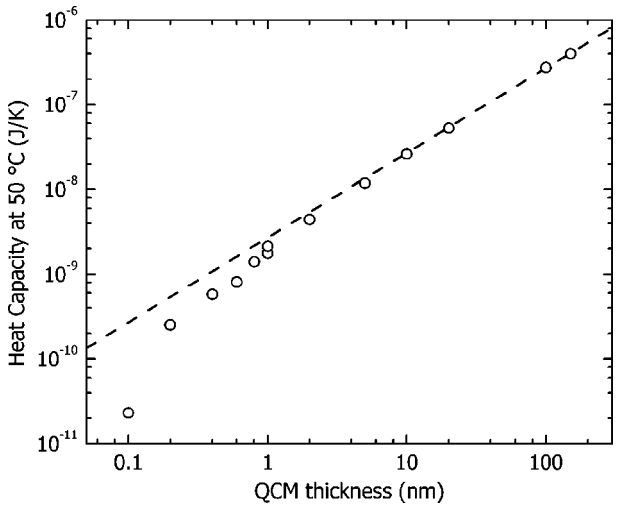

FIG. 6. Heat capacity as a function of thickness measured by the QCM. The dashed line represents the expected value calculated using bulk values for $\overline{c_P}$, ρ_S, and the area of the deposited film. There is a decrease in C_P, showing the difference in sticking between the initial SiN_x surface of the calorimeter and the Bi-coated QCM.

The latent heat of fusion H_m can be calculated from the heat-capacity information by integrating the area under the melting peak.[10] Measured H_m and T_m, along with the bulk values for each, are shown in Figs. 8(a) and 8(b) as functions of the film thickness for 23 films. The film thickness was determined by using m as determined by Eq. (4), ρs, and the area of the deposited film (2.46 mm^2).

Since the calorimetry is done *in situ* with the Bi deposition, and because the measurement is so fast, it is possible to do calorimetry during the growth of the film.[20] This is shown in Fig. 7. Here, calorimetric scans are taken at 1-s intervals, during ~180 s of Bi deposition. The total deposition according to the QCM was 2 nm, but the C_P and H_m obtained from the calorimetric data are more consistent with a total deposition of ~0.04 nm. This may be due to a difference in the sticking coefficient between the QCM and sensor, as described above, or may be due to the increased time-averaged mean temperature of the sensor.

C. Size-dependent melting

The melting point of Bi decreases as the thickness of the Bi film decreases, as shown in Fig. 8(b). To fully quantify the size effects, we directly relate the radius of the Bi particles as determined by TEM analysis to the melting temperature obtained by calorimetry. The results of single-evaporation experiments are now considered. Eight Bi films with nominal thicknesses between 0.3 and 10 nm were measured calorimetrically and with TEM, as described above. For each film, a relationship between T_m and r was determined using the mapping procedure described in our previous work.[10] As can be seen from the results in Fig. 9, as the film thickness increases, the melting temperature trends toward T_m^{bulk}.

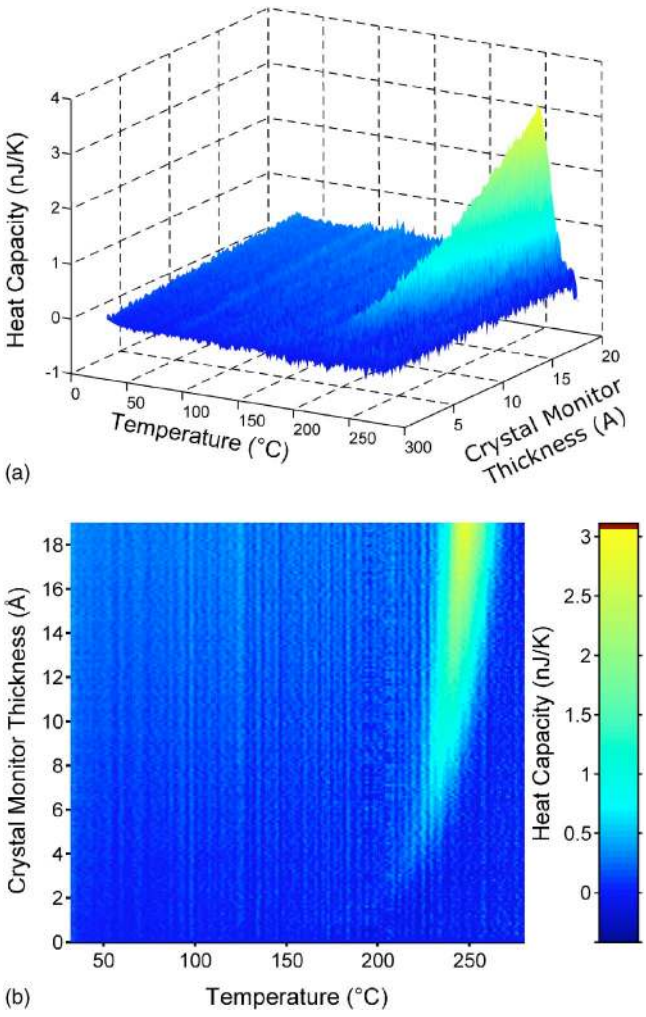

FIG. 7. Real-time calorimetry taken simultaneously with deposition. A constant, slow (~0.1 nm/min) evaporation rate was established, and calorimetric scans taken at 1-*s* intervals. The shutter was opened, and 2 nm (per the QCM) was deposited onto the sensor, simultaneous with the calorimetric scans. This figure shows the heat capacity as the evaporation proceeded.

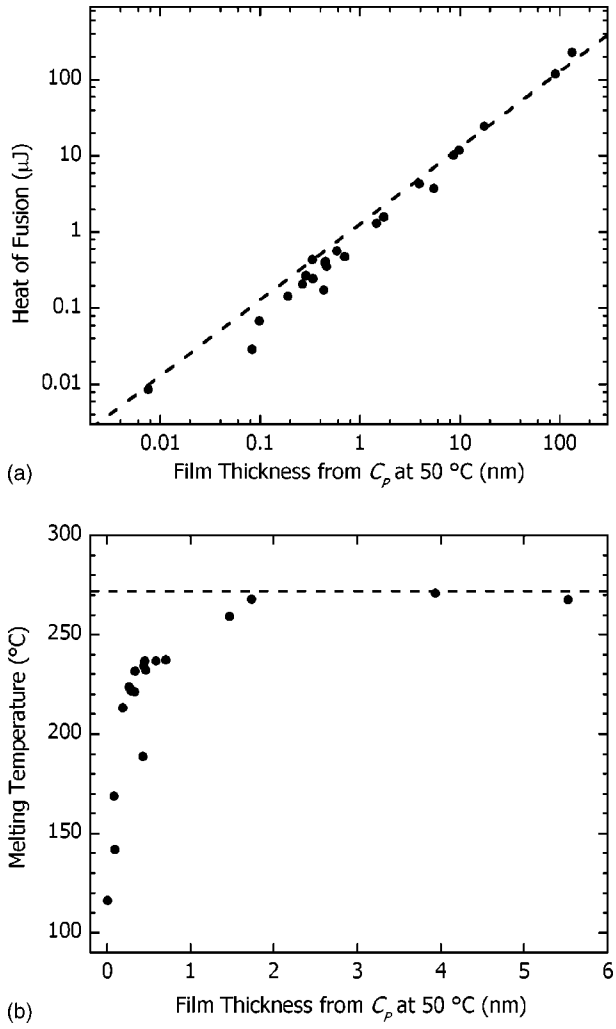

FIG. 8. Heat of fusion and melting temperature for a series of Bi films. (a) Heat of fusion as a function of film thickness for 23 different samples. Film thickness was calculated from the measured C_P, bulk ρ_S, and the area of the film. The bulk heat of fusion is shown by the dashed line. (b) Melting temperature for some of the thinner films, showing a decrease for thin films with small particles.

The results for these films can also be seen in Fig. 10, along with the data reported by Allen *et al.*[6] and Peppiatt.[5] Also shown in that figure is the $T_m(r)$ relationship fitted by Allen *et al.* using the HMM.

IV. DISCUSSION

The size-dependent nature of melting temperature for Bi particles is clearly apparent in our experiments. The quantitative dependence of T_m on r that we obtain, however, is not consistent with the theory. According to Eq. (1), T_m should show a linear dependence on $1/r$. In Fig. 9, however, $T_m(r)$ is approximately constant to T_m^{bulk} for particles above ~7 nm in radius [i.e., $(1/r) \leqslant 0.17\ \text{nm}^{-1}$]. The $T_m(r)$ relation as predicted by Allen *et al.* is shown as a dashed line in Figs. 9 and 10. Our points lie ~50 K above this line, far greater than the experimental error (±5 K). A linear fit to the points below 7 nm, however, has almost the same slope as obtained by Allen *et al.* for $T_m(r)$. We discuss the difference between the theory and our experimental results in terms of thermodynamic effect (i.e., a size-dependent crystal structure) and kinetic effects (i.e., superheating).

A. Crystal structure

Crystal structure can differ from the bulk structure for small particles. Such size-dependent transitions have been observed in In,[24] Si,[25] and Cr,[26] as well as other metals. Since small particles have a high curvature, the surface tension of a solid-vapor or liquid-vapor interface acts as a significant pressure on the particle. At elevated pressures, there are at least six different phases of solid, bulk Bi, and possibly multiple liquid phases.[27] If the pressure on a particle due to surface forces were large enough, the particle would be expected to undergo a phase change. Using bulk values for σ_{LV}, we estimate the surface pressure on a 1-nm radius particle to be 0.8 GPa, whereas bulk Bi requires ~2-GPa pressure to transform from the rhombohedral structure of Bi I to the body-centered-monoclinic structure of Bi II.[27] In addition, a small reduction in the c/a lattice parameter ratio has been suggested for Bi particles below ~4 nm in radius but may not correspond to a crystal structure change.[24]

Other investigators have used high-resolution TEM and reported that very small Bi supported particles exhibited the

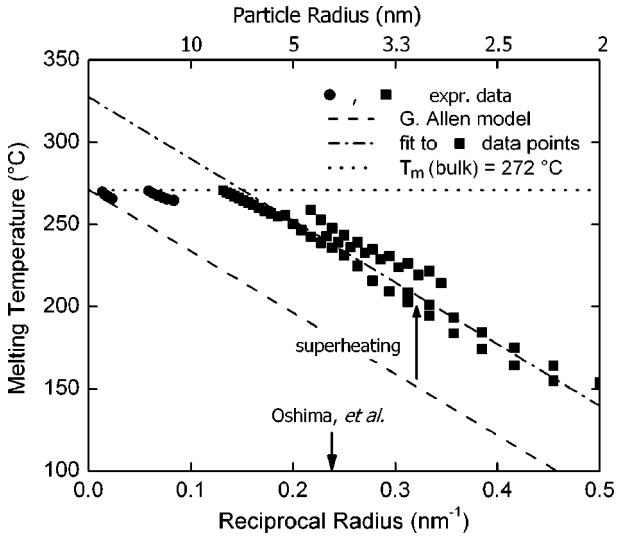

FIG. 9. Melting temperatures as functions of particle sizes, using eight films with nominal thicknesses between 0.3 and 10 nm. The dotted line is T_m^{bulk} for Bi, 271 °C. The dashed line shows the expected $T_m(r)$ behavior calculated from the values using the HMM model and surface energies according to G. Allen *et al.* (Ref. 6). The dash-dot line is a linear fit to the squares. The experimental values for $T_m(r)$ are obtained using the mapping procedure described in Ref. 10.

bulk crystal structure, but that particles above 4.2 nm in radius exhibited a combination of the bulk rhombic and cubic crystal structures.[28] We could not confirm these results, but this may be due to the *ex situ* nature of our TEM examinations, which introduced oxidation and contamination to the samples. This effect was also not found in cluster beam experiments on unsupported Bi nanoparticles between 2- and 5-nm radius.[29]

B. Superheating

The unexpected behavior seen in Fig. 9 can also be explained if the Bi is superheated above its melting temperature. Super*cooling* is commonly observed in the solidification of metals, polymers, and other material systems. We also observe this in Bi. For example, a 150-nm Bi film melts at T_m^{bulk} but solidifies at 165 °C, 107 °C below T_m^{bulk}. The cooling rate at the point where solidification began was 600 K/s. Super*heating*, on the other hand, is not easily observed in metallic systems.

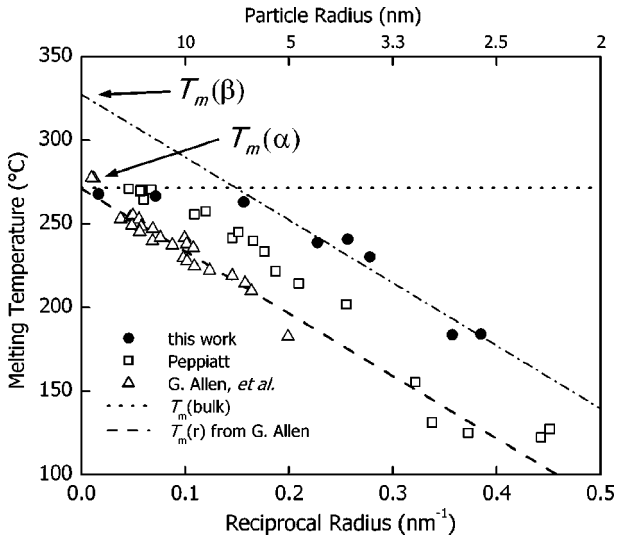

FIG. 10. Comparison of our work with that from two other researchers. The dotted line is T_m^{bulk} for Bi, 271 °C. The dashed and dash-dot lines are the same as in Fig. 9. For clarity, only one point (the media) is shown for each of the eight films from this work.

TABLE II. Experimentally observed superheating of various elements, both embedded in a matrix and freestanding.

Material	Matrix	T_m^{bulk} (K)	Degree of superheating (K)	Ref.
Material embedded in a matrix				
Ag	Au	1234	25	38
Ga	H_2O	301	0.12	39
In	Al	430	29	40
Pb	C	601	140	41
Pb	Al	601	67	42
Pb	Al	601	20	43
Sn	C	505	265	41
Sn	Sn	505	2	5
Freestanding (i.e., nonembedded) material				
Bi	···	545	10	32
Bi (0001)	···	545	90[a]	33
In (111)	···	430	73[a]	44
Pb	···	601	3	45
Pb	···	601	2	46
Pb (111)	···	601	120[a]	34 and 47

[a]Measured at $\sim 10^{11}$ K/s.

Supercooling can occur because, in homogeneous crystallization, there is a barrier to the nucleation of the solid due to the creation of a solid-liquid interface. For melting (which generally proceeds from a free surface or interface), there should be no nucleation barrier to the formation of a liquid, since the solid-vapor interface is generally of higher energy than the sum of the liquid-vapor and solid-liquid interfaces (i.e., $\sigma_{\text{SV}} > \sigma_{\text{SL}} + \sigma_{\text{LV}}$). Thus, it is favorable for a liquid layer to exist between a solid and its vapor at T_m. In other words, the melt of a metal should entirely wet the solid, and superheating should not be possible.[30] Surface-initiated melting is preferred over melting initiated in the body of the crystal, because the latter does have an energetic barrier associated with it due to the strain of forming a liquid nucleus inside a solid matrix.[31]

Contrary to this theory, it has been reported that it is possible to heat a metal above T_m^{bulk}. Generally speaking, superheating is possible if and when the formation of a liquid layer at the surface can be hindered. The simplest way of doing this is by embedding the material in a matrix of a different material, generally of higher melting temperature. Some examples of this are seen in the first part of Table II.

Cases of superheating where there exists a free surface are given in the second part of Table II. Thus, there is a barrier to nucleation of the melt for some materials, whether in the bulk or in the form of nanoparticles.

This phenomenon of superheating where there exists a free surface has previously been reported in Bi.[5,32] In one case, Bi particles were heated to 7 K above T_m^{bulk} before they melted. A time delay in melting was also observed; particles

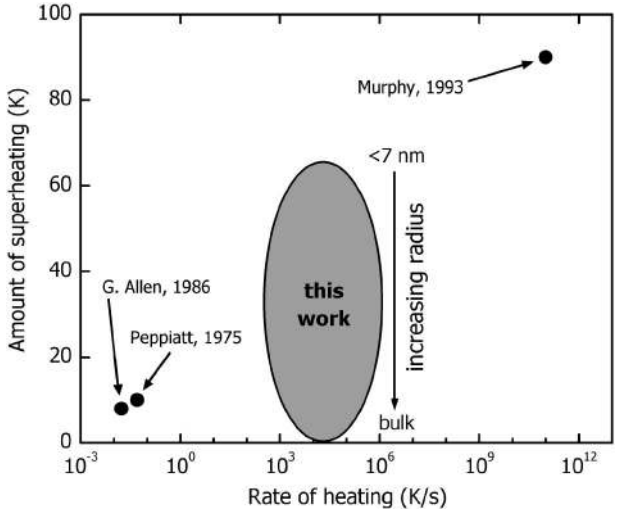

FIG. 11. Amount of superheating found by different researchers for Bi. At low rates, only a few degrees of superheating have been previously observed. At very high rates, the amount of superheating approaches 90 K. Note that the superheating for G. Allen *et al.*, Peppiatt, and Murphy *et al.* is above T_m^{bulk}, while for this work it is above the $T_m(r)$ calculated from Eq. (1). The work of Murphy *et al.* was on a bulk, (0001)-oriented, Bi single crystal; all other work was on Bi nanoparticles.

of a given size did not melt instantaneously at a particular temperature but after a certain period of time they would melt. The time delay was a characteristic of the melting temperature (and therefore, presumably, particle size). Lower temperatures (smaller particles) had a larger characteristic time delay than higher temperatures (larger particles). The particles in this study ranged from 8 to 15 nm in radius.

Allen *et al.*[6] also noticed this phenomenon in 1986, with a superheating of 8 K for large particles ($r>50$ nm). This study included four materials, Bi, In, Pb, and Sn, but the superheating effect was only observed for Bi. Allen *et al.* attributed this to an unknown surface effect which inhibited the formation of a liquid layer at the surface of a particle.

The heating rates used by these two investigators were low, 1–3 K/min, and on the order of those used in traditional differential scanning calorimetry (DSC). More recently, superheating of even bulk Bi single crystals has been observed using ultrafast heating[33] ($\sim 10^{11}$ K/s). This method was used to superheat a Bi (0001) crystal by 90 K. A Pb (111) surface was also superheated by 120 K, but a Pb (110) surface could not be superheated.[34,35] Figure 11 shows the heating rates and measured superheating values in cases where superheated Bi was reported.

Based on only the results discussed above, it is clear that it is possible to heat some metals above their bulk melting temperatures, at least briefly. The question remains whether this superheated state is thermodynamically stable or somehow kinetically trapped in the solid state.

Quasiliquid layers have been observed on micron-sized Sn and In particles below T_m^{bulk}.[14] Melting for these particles is a smooth transition; the surface of a faceted particle roughens, and the liquid layer grows. On Bi particles, however, the facets remain until the entire particle melts all at once, suggesting that there is either no liquid layer, or a thin layer is present but cannot grow below T_m.[13]

TABLE III. Calculated Hamaker constants for several materials (see Ref. 37). The calculation was performed using frequency-dependent, complex dielectric functions.

Material	H ($\times 10^{-21}$ J)
Pb	0.3
Al	0.56
Au	0.85
Bi	<-1.3
Ge	−4.6

C. Hamaker constant

The Hamaker constant H describes the material-dependent component of long-range, dispersive forces between particles and interfaces.[36] It can be calculated from the frequency-dependent dielectric constant of the materials involved. In most cases, H is positive, meaning that there is a repulsive interaction between the solid-liquid interface and the liquid-vapor interface. If the liquid is more conducting than the solid, however, H will be negative and the interaction between the two interfaces will be attractive.[37] Calculated Hamaker constants for some solid-liquid-vapor material systems can be seen in Table III.

Bi and Ge are unusual in that they have a negative H. This is because solid Bi is a semimetal, while liquid Bi is metallic and also because solid Ge is a semiconductor, while liquid Ge is metallic. The effect of this negative H is that there is an attractive force between the liquid-solid and liquid-vapor interfaces on a surface-melted particle. This creates an energetic barrier to the formation of a liquid layer and prevents its formation and/or growth.

This suggests that the $T_m(r)$ relation in Eq. (1) may still hold true, but, because of the high heating rates used here, there is not enough time for melting to proceed.

V. SUMMARY

We have investigated the melting of small Bi particles using a nanocalorimetric technique. Average particle size below a threshold was found to increase linearly with deposition thickness and increase rapidly above it. Small particles were found to melt beneath T_m^{bulk} but above the expected $T_m(r)$. This discrepancy is attributed to superheating due to the suppression of surface melting.

ACKNOWLEDGMENTS

This work was funded under National Science Foundation DMR 0108694 and the American Chemical Society's Petroleum Research Fund Grant No. 33580-AC7. This work was performed in part at the Cornell Nanoscale Science & Technology Facility (a member of the National Nanofabrication Users Network) which is supported by the National Science Foundation under Grant No. ECS-9731293, its users, Cornell University and industrial affiliates. Microanalysis was carried out in the Center for Microanalysis of Materials,

University of Illinois, which is partially supported by the U.S. Department of Energy under Grant No. DEFG02-91-ER45439.

[1]J. P. Issi, Aust. J. Phys. **32**, 585 (1979).
[2]E. I. Rogacheva, S. N. Grigorov, O. N. Nashchekina, S. Lyubchenko, and M. S. Dresselhaus, Appl. Phys. Lett. **82**, 2628 (2003).
[3]J. Heremans, C. M. Thrush, Y. M. Lin, S. Cronin, Z. Zhang, M. S. Dresselhaus, and J. F. Mansfield, Phys. Rev. B **61**, 2921 (2000).
[4]M. S. Dresselhaus *et al.*, Mater. Sci. Eng., C **C23**, 129 (2003).
[5]S. J. Peppiatt, Proc. R. Soc. London, Ser. A **345**, 401 (1975).
[6]G. L. Allen, R. A. Bayles, W. W. Gile, and W. A. Jesser, Thin Solid Films **144**, 297 (1986).
[7]P. Pawlow, Z. Phys. Chem., Stoechiom. Verwandtschaftsl. **65**, 545 (1909).
[8]P. R. Couchman and W. A. Jesser, Nature (London) **269**, 481 (1977).
[9]P. R. Couchman and C. L. Ryan, Philos. Mag. A **37**, 369 (1978).
[10]M. Zhang *et al.*, Phys. Rev. B **62**, 10548 (2000).
[11]M. Schmidt and H. Haberland, C. R. Phys. **3**, 327 (2002).
[12]R. S. Berry, Sci. Am. **263**, 68 (1990); R. S. Berry, Nature (London) **393**, 212 (1998); R. S. Berry, J. Chem. Soc., Faraday Trans. **86**, 2343 (1990); R. S. Berry, D. J. Wales, Phys. Rev. Lett. **63**, 1156 (1989); D. J. Wales and R. S. Berry, Phys. Rev. Lett. **73**, 2875 (1994); D. J. Wales and R. S. Berry, J. Chem. Phys. **92**, 4473 (1990).
[13]A. Pavlovska, D. Dobrev, and E. Bauer, Surf. Sci. **286**, 176 (1993).
[14]A. Pavlovska, D. Dobrev, and E. Bauer, Surf. Sci. **314**, 341 (1994).
[15]Y. Lereah, R. Kofman, J. M. Penisson, G. Deutscher, P. Cheyssac, T. Ben David, and A. Bourret, Philos. Mag. B **81**, 1801 (2001).
[16]E. A. Olson, M. Yu. Efremov, M. Zhang, Z. S. Zhang, and L. H. Allen, J. Microelectromech. Syst. **12**, 355 (2003); M. Yu. Efremov, E. A. Olson, M. Zhang, S. Lai, F. Schiettekatte, Z. S. Zhang and L. H. Allen, Thermochim. Acta **412**, 13 (2004). M. Yu. Efremov, E. A. Olson, M. Zhang, F. Schiettekatte, Z. S. Zhang, and L. H. Allen, Rev. Sci. Instrum. **75**, 179 (2004).
[17]A. Zangwill, *Physics at Surfaces* (Cambridge University Press, Cambridge, 1988).
[18]S. L. Lai and L. H. Allen, presented at the Fourth International Symposium on Quantum Confinement: Nanoscale Materials, Devices, and Systems, Electrochemical Society, Montreal, Quebec, Canada, 4–9 May 1997 (unpublished).
[19]E. A. Olson, University of Illinois at Urbana-Champaign, 2003.
[20]M. Zhang, M. Y. Efremov, E. A. Olson, S. Zhang, and L. H. Allen, Appl. Phys. Lett. **81**, 3801 (2002).
[21]D. Cahill (private communication).
[22]D. Cahill (private communication).
[23]D. R. Lide, *CRC Handbook of Chemistry and Physics*, 82nd ed. (CRC, New York, 2001).
[24]A. Yokozeki and G. D. Stein, J. Appl. Phys. **49**, 2224 (1978).
[25]D. K. Yu, R. Q. Zhang, and S. T. Lee, Phys. Rev. B **65**, 245417 (2002).
[26]S. H. Huh, H. K. Kim, J. W. Park, and G. H. Lee, Phys. Rev. B **62**, 2937 (2000).
[27]A. G. Umnov, V. V. Brazhkin, S. V. Popova, and R. N. Voloshin, J. Phys.: Condens. Matter **4**, 1427 (1992).
[28]Y. Oshima, K. Takayanagi, and H. Hirayama, Z. Phys. D: At., Mol. Clusters **40**, 534 (1997).
[29]A. Wurl, M. Hyslop, S. A. Brown, B. D. Hall, and R. Monot, Eur. Phys. J. D **16**, 205 (2001).
[30]J. H. Holloman and D. Turnbull, Prog. Met. Phys. **4**, 333 (1953).
[31]K. Lu and Y. Li, Phys. Rev. Lett. **80**, 4474 (1998).
[32]M. Blackman, S. J. Peppiatt, and J. R. Sambles, Nature (London), Phys. Sci. **239**, 61 (1972).
[33]E. A. Murphy, H. E. Elsayed-Ali, and J. W. Herman, Phys. Rev. B **48**, 4921 (1993).
[34]J. W. Herman and H. E. Elsayed-Ali, Phys. Rev. Lett. **69**, 1228 (1992).
[35]J. S. Herman and H. E. Elsayed-Ali, Phys. Rev. Lett. **68**, 2952 (1992).
[36]J. N. Israelachvili, *Intermolecular and Surface Forces*, 2nd ed. (Academic, London, 1991).
[37]X. J. Chen, A. C. Levi, and E. Tosatti, Nuovo Cimento Soc. Ital. Fis., D **13**, 919 (1991).
[38]J. Daeges, H. Gleiter, and J. H. Perepezko, Phys. Lett. A **119**, 79 (1986).
[39]J. Jach and F. Sebba, Trans. Faraday Soc. **50**, 226 (1954).
[40]D. L. Zhang and B. Cantor, Acta Metall. Mater. **39**, 1595 (1991).
[41]F. Banhart, E. Hernandez, and M. Terrones, Phys. Rev. Lett. **90**, 185502 (2003).
[42]L. Grabaek, J. Bohr, E. Johnson, A. Johansen, L. Sarholt-Kristensen, and H. H. Andersen, Phys. Rev. Lett. **64**, 934 (1990).
[43]S. Q. Xiao, E. Johnson, S. Hinderberger, A. Johansen, K. K. Bourdelle, and U. Dahmen, J. Microsc. **180**, 61 (1995).
[44]B. Lin and H. E. Elsayed-Ali, Surf. Sci. **498**, 275 (2002).
[45]J. J. Metois and J. C. Heyraud, J. Phys. (Paris) **50**, 3175 (1989).
[46]G. D. T. Spiller, Philos. Mag. A **46**, 535 (1982).
[47]J. W. Herman and H. E. Elsayed-Ali, Phys. Rev. B **49**, 4886 (1994).